JMEPEG (2017) 26:2417–2422
DOI: 10.1007/s11665-017-2657-z

1059-9495/$19.00

Pressureless Sintering of Mo-Si-B Alloys with Fe Additive

Gaoyuan Ouyang, Pratik K. Ray, Matthew J. Kramer, and Mufit Akinc

(Submitted November 1, 2016; in revised form February 9, 2017; published online April 11, 2017)

The sintering behavior of Mo-Si-B alloys with iron as a sintering additive was investigated. The addition of small amounts of Fe effectively enhanced the densification of Mo-Si-B at temperatures below 1900 °C. The addition of 5 at.% Fe resulted in nearly full densification (97.0% of theoretical density) when sintered at 1750 °C for 2 h, while the unmodified Mo-Si-B alloy could be densified to only 66.8% of its theoretical density under these conditions. Addition of 0.5 at.% Fe and 2 at.% Fe increased the degree of densification of Mo-Si-B by 15.4 and 17.0%, respectively, and led to nearly full densification at 1900 and 1850 °C, respectively. Fe-Si-B eutectic liquid was formed at low temperatures and disappeared at high temperatures. We propose that the addition of Fe led to the formation of a transient liquid, facilitating liquid-phase sintering of the powder compacts.

Keywords EDS, intermetallics, liquid-phase sintering, Mo-Si-B, pressureless sintering, SEM, transition metal silicides, ternary silicide borides, XRD

1. Introduction

Molybdenum silicides have been considered as potential candidates for ultra-high-temperature application as early as 1950 (Ref 1). These materials stand out because of their high melting temperatures (above 2000 °C) and their ability to form a protective silica glass at high temperatures. Among these materials, $MoSi_2$ has been studied extensively and reviewed by Yao et al. (Ref 2). It proved to be a good candidate as a high-temperature material because of its high melting point (2050 °C), good oxidation resistance at elevated temperatures, and moderate density (6.24 g cm^{-3}). However, its application is limited by low creep strength at high temperatures, pesting oxidation below 1000 °C, and poor fracture toughness. Akinc et al. explored the doping of boron in Mo_5Si_3 intermetallic (Ref 3). A significant improvement in oxidation resistance and creep resistance was reported when boron was added. Recent efforts focus on eliminating the A15 (Mo_3Si) phase by alloying additions (Ref 4), thus opening up a Mo-Mo_5SiB_2-Mo_5Si_3 phase field. Both Nb (Ref 5) and W (Ref 6) were found to be suitable for the destabilization of A15 phase. Moreover, W additions likely to further increase the melting temperatures of Mo-Si-B alloys.

Densification of Mo-Si-B composites is difficult because of their high melting temperatures. In most studies, Mo-Si-B composites were synthesized by arc melting of the elemental components (Ref 7). However, as Rioult et al. (Ref 8) demonstrated, arc melting cannot produce homogenous microstructures because of the differential cooling rates involved. Microstructural inhomogeneity is exacerbated when larger parts are cast. Furthermore, microstructural features were seen to have a strong effect on the oxidation behavior. Mo-Si-B composites were sintered to nearly full density (about 95% or higher) by hot pressing pressureless sintering (Ref 4, 9), hot isostatic pressing (HIP) (Ref 10), or field-assisted sintering technique (FAST) (Ref 11). However, this approach requires either very high pressures (50 MPa for FAST, 200 MPa for HIP) or very high temperatures, and the densification depends heavily on the compositions with metal-rich composition tending to have higher densification. Middlemas and Cochran (Ref 12) developed a nitride-based reaction sintering route that achieved 94% theoretical density at 1600 °C by pressureless reactive-sintering. Although the sintering temperature was significantly lowered by this process, it was limited Mo-Mo_3Si-Mo_5SiB_2 phase field in the Mo-Si-B ternary. Most notably, the generation of N_2 gas according to the nitride-based chemical reaction made 100% densification impossible. In fact, further hipping was required and reported to achieve full densification. Pressureless sintering is simpler and less expensive than hot pressing because it does not require a complex pressure apparatus and the process is capable of synthesizing near net-shaped components, eliminating the cost of mechanical machining after densification. However, solid-state pressureless sintering requires small particle sizes and high sintering temperatures.

The sintering temperature may be reduced by the choice of an appropriate sintering aid. The purpose of sintering aids is to either reduce the activation energy needed for sintering or increase the mass diffusion rate. In this study, we investigated the efficacy of Fe as a sintering aid for pressureless sintering of Mo-Si-B. According to Poletti and Battezzati (Ref 13), there is a ternary eutectic at Fe-8Si-18B (at. %) composed of BCC Fe, Fe_3B, and $Fe_2Si_{0.4}B_{0.6}$ at 1061 °C in Fe-Si-B system. Hence, addition of Fe to Mo-Si-B is likely to facilitate liquid-phase sintering at temperatures above the eutectic temperature; Fe addition may also enhance the oxidation resistance of Mo-Si-B. According to Sossaman et al. (Ref 14), the oxidation resistance of Mo-Si-B was improved when a small amount of Fe was added. They showed that Fe behaved like a glass modifier and enhanced the fluidity of the protective borosilicate scale, which ensured more efficient surface coverage.

Gaoyuan Ouyang, Pratik K. Ray, Matthew J. Kramer, and **Mufit Akinc**, Department of Material Science and Engineering, Iowa State University, Ames, IA 50011 and Division of Materials Science and Engineering, Ames Laboratory, Ames, IA 50011. Contact e-mail: gaoyuan@iastate.edu.

2. Materials and Methods

Nominal compositions of Mo-20Si-10B-xFe (x = 0, 0.5, 2, 5; all compositions are in at.% unless noted otherwise) were chosen for this work. Elemental Mo powder (99.9%, 3-7 μm, Johnson Matthey), Si powder (99.9985% (metals basis), 1-5 μm, Alfa Aesar), B powder (99%, 44 μm, Cerac), and Fe powder (98+%, 1-3 μm, Alfa Aesar) were properly weighed and mixed together in a SPEX 8000 mixer/shaker mill (SPEX SamplePrep LLC) in argon atmosphere for 30 min. The powders were uniaxially pressed into cylindrical pellets (~12 mm diameter, ~6 mm height) by a Carver Laboratory Press (Model:3393, Carver Inc.). They were further compacted by cold isostatic pressing at 300 MPa. The green densities at this stage ranged from 67-69%. Among these, Fe-containing samples have slightly higher green densities. The pellets were then sintered at different temperatures (1200, 1650, 1750, 1850, 1900, 1925 °C) for different intervals (2-6 h) in an atmosphere of flowing ultra-high-purity argon in alumina crucibles in a tungsten mesh furnace (Model: M60, Centorr associate Inc.). The heating and cooling rates were controlled at 20 °C min^{-1}.

Bulk densities of the samples were measured using the Archimedes technique post-sintering according to ASTM standard B962-13. Theoretical densities were obtained by dividing the total molar mass of the constituent phases (weighted according to their phase fraction) by the total molar volume of the phases (weighted according to their phase fraction) as shown in Eq 1:

$$\rho_{th} = \frac{f_{A15} \times M_{A15} + f_{T2\times} M_{T2}}{f_{A15\times} \frac{M_{A15}}{\rho_{A15}} + f_{T2\times} \frac{M_{T2}}{\rho_{T2}}} \quad \text{(Eq 1)}$$

Here, ρ_{th} represents the theoretical density; f_{A15} and f_{T2} are the phase fractions of the A15 and T2 (Mo_5SiB_2) phases, respectively, as determined by lever rule in Mo-Si-B isotherm at 1600 °C (Ref 7); M_{A15} and M_{T2} are the molar weights of A15 and T2; and ρ_{A15} and ρ_{T2} are the densities of A15 and T2. Relative densities were estimated by dividing the bulk densities by the true densities. The densities reported were averaged over at least three samples, and the standard deviation was found to be less than 1%. Microstructure analysis was carried out using a scanning electron microscope (SEM) (5910LV, JEOL Ltd.), which was equipped with an energy-dispersive spectrometer (EDS) (Noran Vantage, Noran Instruments, Inc.); polished sample cross sections were used for SEM investigations. For chemical analysis of the phases, wavelength-dispersive spectroscopy (WDS) (8200, JEOL Ltd.) with Mo-L, Fe-K, Si-K, and B-K lines at a 15 kv accelerating voltage and a 12 nA beam current was employed. Phase analysis was carried out using a x-ray diffractometer (Philips PANalytical X'pert Pro, PANalytical) using Cu K_α radiation with a double-bent monochromator. Samples were crushed, ground, and sieved to 45 μm before collecting x-ray data. The x-ray data were Rietveld-refined using the GSAS software (Ref 15) to obtain lattice parameters and phase fractions.

3. Results

According to the Mo-Si-B phase diagram (Ref 7), a nominal composition of Mo-20Si-10B yields exclusively Mo_3Si and Mo_5SiB_2 phases in thermodynamic equilibrium at 1600 °C. Based on the lever rule, the phase fractions of A15 and T2 are 0.6 and 0.4, respectively. This is consistent with the refined phase fractions of the sintered samples as shown in Table 2.

Figure 1 shows the densification of the Mo-Si-B-(Fe) composites as a function of Fe content and sintering temperature after 2 h of sintering. In general, it can be seen that an increase in sintering temperature resulted in an increase in densification (the samples containing 5% Fe being the only exception). Similarly, for a given temperature, increasing Fe content improved densification.

Table 1 shows the collected data as well as similar data for longer sintering periods. As expected, dependence of densification on sintering time is relatively weak. At lower temperatures, the relative density of sintered sample fell below the relative density of the green compact. This is probably due to the poorer packing efficiency of A15 and T2 after sintering than Mo, Si, and B powder compacts before sintering. In addition, the theoretical density increased from 7.87 g cm^{-3} for the powder compacts to 8.83 g cm^{-3} for the sintered body.

Figure 2 shows SEM micrographs depicting the porosity level and phases present in the alloys. The darkest round structures are pores. Pore size and number of pores decreased with increasing Fe addition, indicating an increase in densification as the Fe content is increased from zero to 2 at.%. This is probably resulted from an increase in fraction of liquid during the sintering. According to Fe-Si-B phase diagram (Ref 13), the eutectics occur at relatively higher Fe content. Therefore, the liquid was formed at Fe-rich region where the initial high Fe content drove the local liquid composition toward the eutectics. Hence, higher Fe addition resulted in a larger liquid fraction during sintering. The phases visible in the micrographs are the Mo-rich solid solution (Mo), A15, and T2, corresponding to the bright, gray, and dark gray features in the micrographs, respectively.

As shown in Fig. 2, the addition of 2 at.% Fe and 5 at.% Fe sintered at 1850 °C resulted in a significant increase in A15 and T2 grain size. The sample with 5 at.% Fe addition exhibited large A15, T2, and (Mo) grains, together with discrete eutectic structures in the phase boundaries. WDS analysis showed that the Fe content in the (Mo), A15, and T2 phases was about 4, 2, and 2 at.%, respectively. In addition, it was detected that the

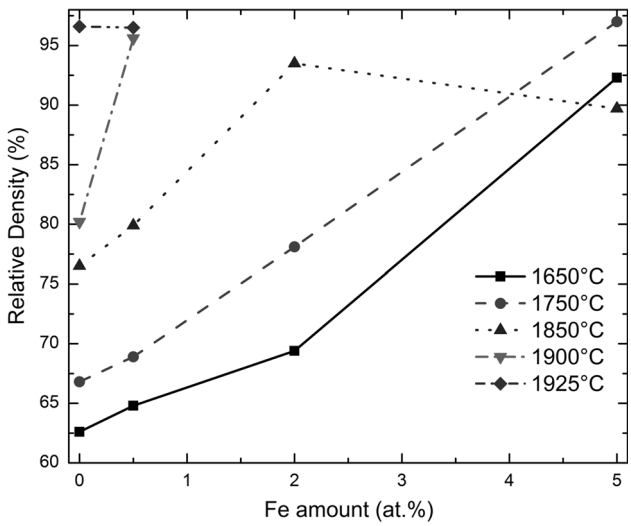

Fig. 1 Relative sintered density of Mo-Si-B alloys as a function of Fe content at several sintering temperatures

Table 1 Relative densities of post-sintered Mo-Si-B-(Fe) composites sintered at different temperatures and time periods

	Relative densities, %						
Fe amount, at.%	**1650 °C 2 h**	**1650 °C 6 h**	**1750 °C 2 h**	**1850 °C 2 h**	**1850 °C 6 h**	**1900 °C 2 h**	**1925 °C 2 h**
0	62.6	63.7	66.8	76.5	81.0	80.2	96.6
0.5	64.8	66.2	68.9	79.9	84.3	95.6	96.5
2	69.4	74.4	78.1	93.5	92.4	…	…
5	92.3	92.9	97.0	89.7	87.0	…	…

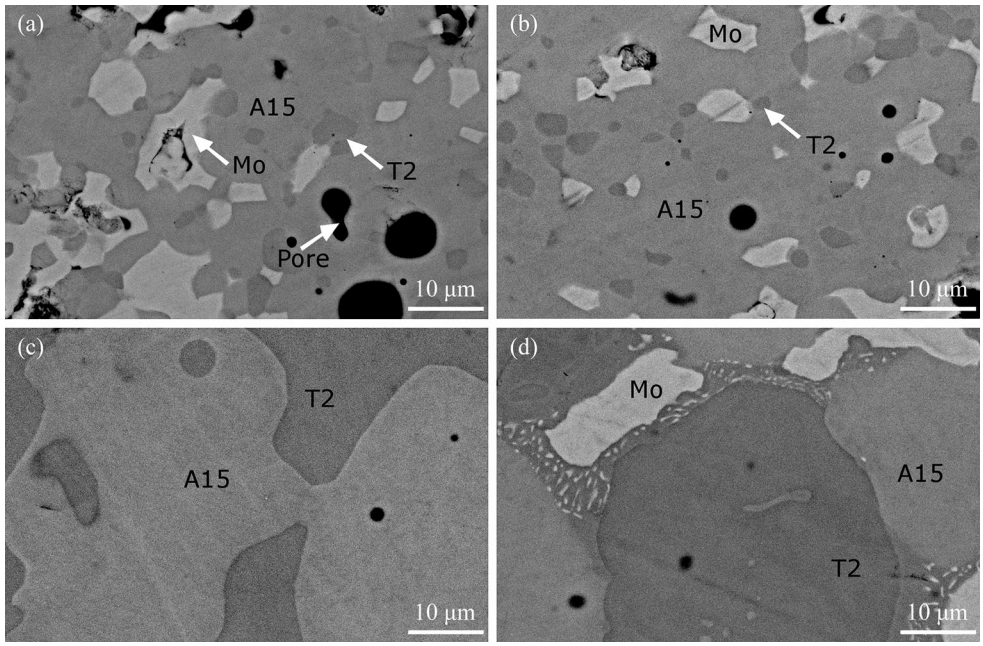

Fig. 2 SEM backscattered images of Mo-Si-B-(Fe) alloys sintered at 1850 °C: (a) 0, (b) 0.5, (c) 2, and (d) 5 at.% Fe addition

eutectic region contained the equivalent of approx. 20 at.% Fe concentration. The eutectic structure was too fine to yield reliable quantitative values of the individual phases from WDS analysis. However, it could be inferred from WDS results that the addition of 5 at.% Fe at sintering conditions of 1850 °C, 2 h, resulted in higher Fe solution into the A15, T2, and (Mo) phases and exceeded their solubility limits (as will be discussed below) and the excess Fe stayed at the (Mo), A15, and T2 interphase areas as eutectic phase.

In addition to SEM and EDS analysis, x-ray diffraction (XRD) was also carried out to study the phases present in the alloys. As expected, A15 and T2 were the major phases. The (Mo) phase was present in very small amounts in the 0 at.% Fe and 0.5 at.% Fe samples, possibly because of the limited mass transportation rate during solid-state sintering, which left a small amount of Mo unreacted. As the Fe content was further increased (2 and 5 at.%), the (Mo) peaks disappeared. The disappearance of (Mo) was possibly caused by the increased Si reactivity, forming A15 and T2 in the presence of a liquid phase. The presence of a liquid phase was also likely to increase the mass transportation rate during the sintering process, which in turn served to better homogenize the composition compared to the zero and 0.5 at.% Fe samples.

Rietveld refinements were carried out on the XRD patterns shown in Fig. 3 to better understand and verify the sintering mechanism. The refinement results are shown in Table 2 (the results for samples with 5 at.% Fe addition are not shown

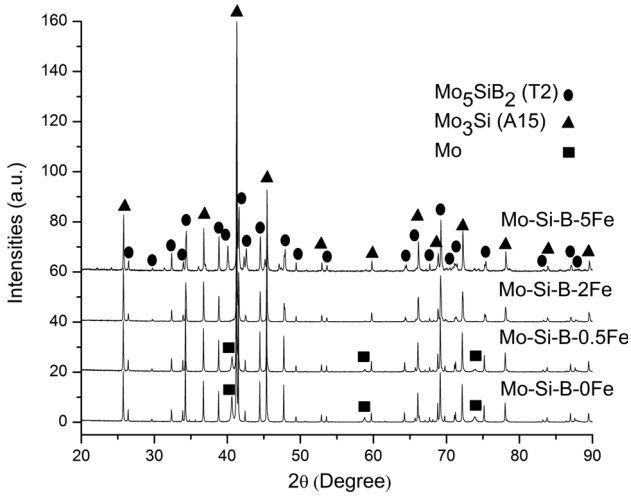

Fig. 3 XRD patterns of Mo-Si-B (Fe) alloys. Samples were sintered for 2 h at 1850 °C. Fe amounts are given in at.%

because high wRp (weighted *R*-factor) values were caused by small, unresolved peaks). The results showed a decrease in lattice parameters of the A15 and T2 phases (lattice parameters for the (Mo) phase are not shown because only very small amounts of (Mo) were present). This can also be seen in the XRD pattern in Fig. 3, where T2 and A15 peaks slightly shifted

Table 2 Rietveld refinement results

Fe in at.%	Wt.%			Lattice parameter, Å			Goodness of fit
	Mo, %	A15, %	T2, %	A15, a	T2, a	T2, c	WR_p
0	6.4	57.0	36.6	4.8979	6.0282	11.0740	0.12
0.5	6.3	61.5	32.2	4.8970	6.0258	11.0726	0.13
2	0.06	64.2	35.2	4.8905	6.0142	11.0662	0.16

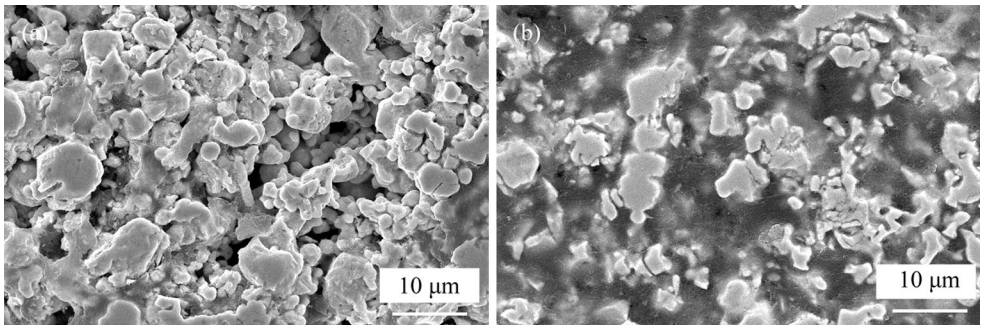

Fig. 4 SEM secondary images of Mo-Si-B-(Fe) alloys sintered at 1200 °C for 6 h: (a) 0 and, (b) 5 at.% Fe addition alloy

to higher angles. The decrease in lattice parameters was caused by the smaller atomic size of Fe (1.26 Å) substituting for a larger Mo (1.39 Å) atom (Ref 16).

In order to ascertain the formation of transient liquid prior to its destabilization, the Fe-free sample and the sample with 5 at.% Fe were sintered at 1200 °C for 6 h. Post-sintering SEM micrographs are shown in Fig. 4. Hardly, any densification was seen in the Fe-free sample at this temperature, as evident with individual particle morphology and interconnected open-pore structure. In contrast, the sample with 5 at.% Fe showed a continuous matrix (dark contrast matrix) in the background. This continuous matrix implied the formation of a low-viscosity liquid that flowed throughout the sample, which was likely to enhance the mass transportation rate during sintering. The EDS spectrum of this dark matrix reflected a high content in Fe, Si, B, and O, which indicated the formation of a Fe-containing liquid phase. This Fe-containing phase probably then interacts with the surface oxygen of the fine starting particles and results in a Fe-Si-B-O liquid around the (Mo)-containing grains.

4. Discussion

According to the liquidus projection phase diagram proposed by Nunes et al. (Ref 17), Mo-Si-B can form a eutectic consisting of Mo, A15, and T2 at the phase equilibria of interest to our investigation. Schneibel et al. (Ref 18) also suggested that Mo-Si-B may form a liquid at a temperature as low as 1927 °C. This possible liquid formation explains the sudden increase in density in Mo-Si-B alloys sintered at 1925 °C compared to those sintered at 1900 °C. The difference between the experimentally measured sintering temperature of 1925 °C and the liquidus temperature of 1927 °C suggested by the literature is within the limits of experiment error.

The Fe-Si-B system is known to have multiple eutectics. Most of these eutectics are found in the Fe-rich region of the phase space. As the powder compact is heated during the initial stage of sintering, small amounts of Si and B around individual Fe particles allow for the formation of a eutectic liquid. This low-viscosity liquid having viscosity values of 6-8 mPa s in the 1302-1502 °C range as suggested by Nakagawa et al. (Ref 19) plays an important role during sintering. As reviewed by German et al. (Ref 20), formation of a liquid would lead to improved densification. However, excessive liquid fractions during the sintering process can also result in a loss of shape, when sintering the Mo-20Si-10B-5Fe sample at 1850 °C.

Poletti and Battezzati (Ref 13) reported the enthalpy change during the eutectic reaction in a number of Fe-Si-B eutectics. Calorimetric experiments showed that the enthalpy change during these eutectic reactions ranged between 13 and 17 kJ mol^{-1}. Calorimetric studies showed that the formation enthalpy for the A15 Mo_3Si was approximately −122 kJ mol^{-1} (Ref 21, 22) or −30 kJ mol^{-1} $atom^{-1}$. Our calculations, using Miedema's model (Ref 23), showed a very close match with these values (−27.3 kJ mol^{-1} $atom^{-1}$). Ab- initio studies on the T2 Mo_5SiB_2 compound by Kim and Park (Ref 24) revealed a formation enthalpy of approximately −43 kJ mol^{-1} $atom^{-1}$. The Mo-Si-Fe phase diagram (Ref 25) shows a maximum of 2 at.% solubility of Fe in the A15 phase, which is consistent with our experimental data (mentioned earlier in this paper). We calculated the formation enthalpy of Fe-substituted Mo_3Si in accordance with Miedema's semi-empirical model (Ref 26-28) and its subsequent extension (Ref 23), and the results are presented in Fig. 5. As clearly seen in the figure, the addition of Fe decreased the formation enthalpy only slightly, indicating the possibility of a marginal stabilization. Besides the A15 phase, the other major phase in the present investigation was the T2 phase. It is known that both, Fe_5SiB_2 and Mo_5SiB_2, crystallize in the I4/mcm space group (Ref 29) with similar lattice parameters (Fe_5SiB_2: $a = 0.5540$ nm, $c = 1.0320$ (Ref 30); Mo_5SiB_2: $a = 0.5998$ nm, $c = 1.1027$ nm (Ref 31)); in fact, the structure prototype for both compounds is Mo_5SiB_2, indicating a possibility of solid solubility between these two phases. A small amount of Fe in the T2 phase in the present investigation ($< 4\%$) was unlikely to reduce the formation enthalpy of T2 drastically. It is expected that with minor Fe additions the thermodynamic

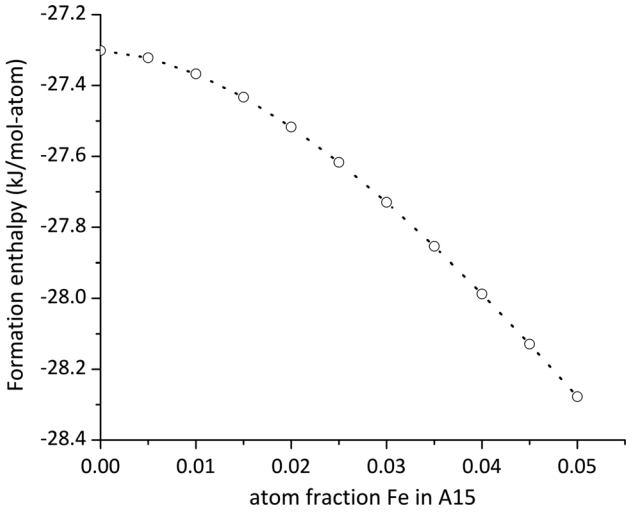

Fig. 5 Formation enthalpy of Fe-substituted Mo_3Si as a function of Fe amount

equilibrium would favor the formation of the A15 and T2 compounds rather than the A15 and T2 compounds along with a Fe-Si-B liquid.

However, the formation of Fe-Si-B eutectics occurs at relatively lower temperatures (<1600 °C). Therefore, it is reasonable to expect the eutectics to form initially, but eventually disappears in reactions with other phase to yield Fe-substituted A15 and T2 phases. This has significant implications for the sintering mechanism in this system. It is suggested that the densification progressed via a transient liquid-phase sintering mechanism. This sintering process involved an initial inter-diffusion between the elemental Mo, Fe, Si, and B, initially leading to the formation of a Fe-Si-B eutectic. This eutectic was probably a transient liquid, which later decomposed. The formation of liquid between the phase boundaries enabled liquid-phase sintering. Solute transport through the liquid and subsequent deposition on the adjacent phases is well-known for liquid-phase sintering (Ref 20). In the present case, it likely involved the transport of Fe atoms, among others, to the adjacent Mo-containing phases, where they dissolved in small amounts in the structure. Dissolution of Fe into Mo-rich phases depleted the Fe content of the liquid. Because the Fe-Si-B eutectic is present in the Fe-rich regions (Ref 13), this resulted in a gradual decomposition of the liquid as the phase assemblage approached thermodynamic equilibrium. Transitional nature of the liquid is extremely important for sintering of this material. If the liquid phase remains as a low melting phase after sintering, it limits the service temperature of the component which defeats the purpose. What is not known at this stage though, is the rate at which eutectic liquid decomposes. It is possible that the decomposition and disappearance of the liquid phase occurs before full densification is realized. If full densification is to be achieved, a more detailed investigation of liquid decomposition kinetics is necessary. Only after that, an optimized densification protocol may lead to fully dense microstructures.

5. Conclusions

The sintering behavior of Mo-Si-B alloys with the addition of Fe was studied. With small amounts of added Fe, the sintering temperature was lowered by 175 °C. Nearly full densification (97.0%) was obtained with 5 at.% of Fe, sintered at 1750 °C. When 2 at.% of Fe was added, only 1850 °C was required to obtain 93.5% densification. When 0.5 at.% Fe was added, 95.6% densification was achieved at a sintering temperature of 1900 °C. In general, addition of Fe had a beneficial effect on the densification behavior of Mo-Si-B alloys, as long as the temperature was maintained below the melting temperature. Formation of a transient liquid is thought to be a possible mechanism behind the enhanced densification. However, further studies are required to ascertain the exact liquids formed during this process, as well as the stability regimes of the liquid vis-à-vis the A15 and the T2 phases.

Acknowledgments

This work was supported by the AFOSR HTAM under contract #FA9550-11-1-201. The authors would like to thank Warren Straszheim for his help in the WDS analyses.

References

1. L. Brewer, A. Searcy, D. Templeton, and C. Dauben, High-Melting Silicides, *J. Am. Ceram. Soc.*, 1950, **33**(10), p 291–294
2. Z. Yao, J. Stiglich, and T.S. Sudarshan, Molybdenum Silicide Based Materials and Their Properties, *J. Mater. Eng. Perform.*, 1999, **8**(3), p 291–304
3. M. Akinc, M. Meyer, M. Kramer, A. Thom, J. Huebsch, and B. Cook, Boron-Doped Molybdenum Silicides for Structural Applications, *Mater. Sci. Eng. Struct. Mater. Prop. Microstruct. Process.*, 1999, **261**(1-2), p 16–23
4. V. Behrani, A. Thom, M. Kramer, and M. Akinc, Microstructure and Oxidation Behavior of Nb-Mo-Si-B Alloys, *Intermetallics*, 2006, **14**(1), p 24–32
5. P.K. Ray, M. Akinc, and M.J. Kramer, Applications of An Extended Miedema's Model for Ternary Alloys, *J. Alloy. Compd.*, 2010, **489**(2), p 357–361
6. P.K. Ray, Y. Ye, M. Akinc, and M.J. Kramer, Effect of Nb and W Substitutions on the Stability of the A15 Mo_3Si Phase, *J. Alloy. Compd.*, 2012, **537**, p 65–70
7. D. Dimiduk and J. Perepezko, Mo-Si-B Alloys: Developing a Revolutionary Turbine-Engine Material, *MRS Bull.*, 2003, **28**(9), p 639–645
8. F. Rioult, S. Imhoff, R. Sakidja, and J. Perepezko, Transient Oxidation of Mo-Si-B Alloys: Effect of the Microstructure Size Scale, *Acta Mater.*, 2009, **57**(15), p 4600–4613
9. M. Meyer, A. Thom, and M. Akinc, Oxide Scale Formation and Isothermal Oxidation Behavior of Mo-Si-B Intermetallics at 600-1000 Degrees C, *Intermetallics*, 1999, **7**(2), p 153–162
10. M. Krüger, S. Franz, H. Saage, M. Heilmaier, J.H. Schneibel, P. Jéhanno, M. Böning, and H. Kestler, Mechanically Alloyed Mo-Si-B Alloys with a Continuous α-Mo Matrix and Improved Mechanical Properties, *Intermetallics*, 2008, **16**(7), p 933–941
11. M. Krüger, D. Schliephake, P. Jain, K.S. Kumar, G. Schumacher, and M. Heilmaier, Effects of Zr Additions on the Microstructure and the Mechanical Behavior of PM Mo-Si-B Alloys, *JOM*, 2013, **65**(2), p 301–306
12. M. Middlemas and J. Cochran, Dense, Fine-Grain Mo-Si-B Alloys from Nitride-Based Reactions, *JOM*, 2008, **60**(7), p 19–24
13. M.G. Poletti and L. Battezzati, Assessment of the Ternary Fe–Si–B Phase Diagram, *Calphad*, 2013, **43**, p 40–47
14. T. Sossaman, R. Sakidja, and J. Perepezko, Influence of Minor Fe Addition on the Oxidation Performance of Mo-Si-B Alloys, *Scripta Mater.*, 2012, **67**(11), p 891–894
15. B. Toby, EXPGUI, a Graphical User Interface for GSAS, *J. Appl. Crystallogr.*, 2001, **34**, p 210–213
16. L. Pauling, Atomic Radii and Interatomic Distances in Metals, *J. Am. Chem. Soc.*, 1947, **69**(3), p 542–553

17. C. Nunes, R. Sakidja, Z. Dong, and J. Perepezko, Liquidus Projection for the Mo-Rich Portion of the Mo-Si-B Ternary System, *Intermetallics*, 2000, **8**(4), p 327–337
18. J.H. Schneibel, C.T. Liu, D.S. Easton, and C.A. Carmichael, Microstructure and Mechanical Properties of Mo-Mo_3Si-Mo_5SiB_2 Silicides, *Mater. Sci. Eng. Struct. Mater. Prop. Microstruct. Process.*, 1999, **261**(1-2), p 78–83
19. K. Nakagawa, T. Kanadani, Y. Mori, and Y. Ishii, The Effect of Jetting Temperature on the Fabrication of Rapidly Solidified Fe-Si-B Systems Alloys Using Single-Roller Melt Spinning, *Mater. Trans.*, 2011, **52**(2), p 196–200
20. R. German, P. Suri, and S. Park, Review: Liquid Phase Sintering, *J. Mater. Sci.*, 2009, **44**(1), p 1–39
21. I. Tomaszkiewicz, G.A. Hope, C.M. Beck Ii, and P.A.G. O'Hare, Thermodynamic Properties of Silicides V. Fluorine-Combustion Calorimetric Determination of the Standard Molar Enthalpy of Formation at the Temperature 298.15 K of Trimolybdenum Monosilicide Mo_3Si, and a Critical Assessment of its Thermodynamic Properties, *J. Chem. Thermodyn.*, 1996, **28**(1), p 29–42
22. H. Fujiwara and Y. Ueda, Thermodynamic Properties of Molybdenum Silicides by Molten Electrolyte EMF Measurements, *J. Alloy. Compd.*, 2007, **441**(1-2), p 168–173
23. L.J. Gallego, J.A. Somoza, and J.A. Alonso, Glass Formation in Ternary Transition Metal Alloys, *J. Phys. Condens. Matter*, 1990, **2**(29), p 6245
24. S. Kim and J. Park, Ab Initio Calculated Thermodynamic Properties of Mo_5SiB_2 Phase and Nb_5SiB_2 Phase, *JOM*, 2013, **65**(11), p 1482–1486
25. G. Inden, Phase Equilibria in Iron Ternary Alloys. By G. V. Raynor and V. G. Rivlin. The Institute of Metals, London 1988. xiii, 485 pp., bound, US $ 129.—ISBN 0-901462-34-9, *Adv. Mater.*, 1990, **2**(1), p 58–59
26. A.R. Miedema, P.F. de Châtel, and F.R. de Boer, Cohesion in Alloys—Fundamentals of a Semi-Empirical Model, *Physica B+C*, 1980, **100**(1), p 1–28
27. A.K. Niessen, F.R. de Boer, R. Boom, P.F. de Châtel, W.C.M. Mattens, and A.R. Miedema, Model Predictions for the Enthalpy of Formation of Transition Metal Alloys II, *Calphad*, 1983, **7**(1), p 51–70
28. H. Bakker, *Enthalpies in Alloys*, Trans-Tech Publishers, The Netherlands, 1998
29. N.F. Chaban and Y.B. Kuz'ma, Phase Equilibria in the Systems Manganese-Silicon-Boron and Iron-Silicon-Boron, *Inorg. Mater.*, 1990, **6**, p 883–884
30. B. Aronsson and G. Lundgren, X-Ray Investigations on Me-Si-B Systems (Me=Mn, Fe, Co).1. Some Features of the Co-Si-B System at 1000 degrees C. Intermediate Phases in the Co-Si-B and Fe-Si-B Systems, *Acta Chem. Scand.*, 1959, **13**(3), p 433–441
31. B. Aronsson, The Crystal Structure of Mo_5SiB_2, *Acta Chem. Scand.*, 1958, **12**(1), p 31–37